Preparation of Xanthan Gum-based Composite Hydrogels with Aligned Porous Structure

Heli Cheng,[a,b,c]* Xu Zhang,[a,c] Jiawei Xu,[a,c] and Sicheng Liu [a,c]

Aligned hydrogels have received increasing attention in tissue engineering and electrochemical fields due to their favorable structure. In this work, xanthan gum-based hydrogels (XGH) with aligned pores were prepared *via* photoinitiated free radical irradiation that used sodium acetate crystals as template. The microstructure, compressive strength, porosity, and absorption capacity of the hydrogel were studied and compared with the non-aligned hydrogels. Scanning electron microscope analysis confirmed the aligned porous structure of the hydrogel. The maximum compressive strength for the aligned hydrogel prepared with 12% acrylamide and 1.5% xanthan gum reached 0.439 MPa at a strain of 95%. Furthermore, aligned XGH exhibited better flexibility than non-aligned hydrogels, as indicated by the Young's compressive modulus. The porosity of the aligned hydrogels ranged from 94.9% to 88.8% as the acrylamide concentration increased from 12% to 20%. Simulated body fluid absorption showed that hydrogels with aligned pores could attain absorption equilibrium within 5 min, and the maximum absorption capacity reached 33.6 g/g for the sample made with 0.5% xanthan gum and 12% acrylamide. In addition, exhibited preferable biocompatibility, as demonstrated by the cytotoxicity test.

Keywords: Xanthan gum; Acrylamide; Composite hydrogel; Aligned structure

Contact information: a: Hubei Provincial Key Laboratory of Green Materials for Light Industry, Hubei University of Technology, Wuhan 430068 China; b: State Key Laboratory of Pulp and Paper Engineering, South China University of Technology, Guangzhou 510640 China; c: School of Materials and Chemical Engineering, Hubei University of Technology, Wuhan 430068 China;
** Corresponding author: pphlcheng@163.com*

INTRODUCTION

Hydrogels are commonly defined as a three-dimensional hydrophilic polymer that is able to absorb and retain a significant quantity of water or biological fluids while maintaining their physical integrity (Hoffman 2012). Since the pioneering work of Wichterle and Lim on the synthesis of the poly(2-hydroxyethylmethacrylate) (pHEMA) hydrogel in 1960, hydrogels have received considerable attention due to their broad applications in biosensors, environment, agriculture, drug delivery, *etc*. (Wichterle and Lim 1960; Drury and Mooney 2003; Lian *et al*. 2018; Song *et al*. 2018).

Generally, the internal morphology of a hydrogel consists of disordered interconnected pores, which can meet the application demands of most occasions. However, in cases like the regeneration of directing axonal or spinal cord, or the porous electrolyte that used for ion transportation, hydrogels with directionally grown, oriented, and controllable porous morphology are more desirable (He *et al*. 2016). Ice templating is one of the simplest ways to fabricate gels with oriented pores. Typically, a precursor solution is immersed in a cold liquid (liquid nitrogen is always used) at a certain rate to

guide the growth direction of ice crystals, where aligned porous hydrogels would be obtained by the removal of the ice crystals *via* freeze drying (Barrow and Zhang 2013; Liu *et al*. 2015). Nevertheless, materials prepared by this method are mechanically brittle. Electrospinning is another way to obtain hydrogel with aligned structure because channels between the spinning fibers are directionally arranged. An aligned hydrogel microfiber with a high elasticity was constructed with a photocrosslinked gelatin methacryloyl by electrospinning technology; the resulting directional porous structure made the hydrogel an efficient scaffold to guide cell migration and axon extension (Chen *et al*. 2019). Needle-like $NaAc \cdot 3H_2O$ crystals with micrometer size and aligned structure could be generated by crystallization of a supersaturated NaAc solution. $NaAc \cdot 3H_2O$ crystals are transparent and similar in appearance to ice crystals. Recently, He *et al*. (2016) successfully fabricated an aligned agarose-gelatin hydrogel with macroporous structure using $NaAc \cdot 3H_2O$ crystal as a template and demonstrated that cells could differentiated and grew along the aligned parallel channels.

Xanthan gum (XG) is a neutral water-soluble heteropolysaccharide secreted by *Xanthomonas campestris* (Katzbauer 1998). In 1969, xanthan gum was approved as a food additive by the United States Food and Drug Administration (FDA) due to its non-toxic and non-sensitizing properties. China has become one of the largest XG producers since 2005 (Bellini *et al*. 2012; Anjum *et al*. 2015; Petri 2015; Kumar *et al*. 2018). The primary structure of the XG polysaccharide includes a D-glucose backbone linked by *β*-1,4 glycosidic bonds with trisaccharide side chains. The chemical structure of the backbone is similar to that of cellulose. The side chains are made up of *β*-D-mannose, 1,4-*β*-D-glucuronic acid, and 1,2-*α*-D-mannose, where the internal 1,2-*α*-D-mannose connects to the main chain at the C-3 position of every other D-glucosyl unit. Most of the internal mannoses are *O*-acetylated at the C-6 position, while nearly one-half of the terminal *β*-D-mannoses are substituted with a 4,6-linked pyruvic acid ketal (Katzbauer 1998; García-Ochoa *et al*. 2000). The secondary structure of xanthan gum is a five-fold rod-like helical structure that is formed by reverse winding of the charged trisaccharide side-chain around the main chain *via* hydrogen bonding and electrostatic forces. This interesting structure protects the main chain of XG from the degradation by acids, bases, and enzymes. It has been reported that XG solution is extremely stable over a wide range of pH values (2 to 11) and temperatures (up to 90 °C) (Lachke 2004). Furthermore, one of the most unusual properties of xanthan gum is its behavior in salt solutions. It has been reported that the viscosity of xanthan gum is insensitive to salt concentration at high salt levels (Muller *et al*. 1986; Rochefort and Middleman 1987).

Besides being widely used as thickener and emulsion stabilizers in the food industry, XG-based materials are also interesting substances to be applied in the biomedical field due to their biocompatible and biodegradable properties (Petri 2015). For example, chitosan-xanthan membranes can be used as wound dressing for the treatment of skin lesions (Bellini 2012). The mixture of konjac glucomannan and xanthan gum can effectively retard cimetidine release from tablet matrices (Fan *et al*. 2008). In this study, XG was selected as the main component to fabricate composite hydrogels with aligned structures and preferably flexibility by adopting $NaAc \cdot 3H_2O$ crystal as template, due to its special structure and properties. The intention of this work was to find a polysaccharide system that could use $NaAc \cdot 3H_2O$ crystal template and also provide a promising material that could be applied as bioscaffold in tissue engineering or as electrolyte in supercapacitors.

EXPERIMENTAL

Materials

Xanthan gum (USP Grade), *N*,*N*'-methylene-bis-acrylamide (MBAA), and 2-hydroxy-4'-(2-hydroxyethoxy)-2-methylpropiophenone (Irgacure 2959) were purchased from the Aladdin Industry Corporation (Shanghai, China). Acrylamide (AM, $CH_2CHCONH_2$) was obtained from the Sahn Chemical Technology Co., Ltd. (Shanghai, China). Dimethyl sulfoxide (DMSO) and anhydrous sodium acetate (NaAc, CH_3COONa) were purchased from the Sinopharm Chemical Reagent Co., Ltd. (Shanghai, China). Sodium acetate trihydrate ($NaAc{\cdot}3H_2O$) was purchased from the Tianjin Bodi Chemical Co., Ltd. (Tianjin, China). Gelatin of medical grade was bought from the Shanghai Baoman Biotechnology Co., Ltd. (Shanghai, China). Other chemicals used were of reagent grade and were used without further purification. Deionized water was used in all experiments.

Preparation of Xanthan Gum-based Hydrogels

Xanthan gum-based hydrogels (XGH) with aligned pores were prepared in 100-mL glass beakers. First, excess NaAc was dissolved in 22.88 g distilled water to obtain a supersaturated solution. Then, 0.3 g gelatin was added to the above solution while mixing with a magnetic stirrer until it completely dissolved at 90 °C. Afterward, 4.5 g AM, 1.125 mL MBAA (20 mg/mL, 0.5 wt% of AM), and 0.135 g photoinitiator (Irgacure 2959, 3 wt% on AM) were added to the as-prepared solution. The mixture was placed in the dark after the photoinitiator was added. After dissolution at 90 °C with stirring, 0.3 g XG and 6 mL DMSO were added to the beaker to result in a total volume of 30 mL. Then, the mixture was stirred at 70 °C until the XG was totally dissolved to obtain a homogeneous solution. Next, the solution was poured into five glass vials. After cooling to room temperature, one grain of $NaAc{\cdot}3H_2O$ was added to each glass vial to induce crystallization. The glass vials were then placed under ultraviolet (UV) light (365 nm) for 2 h for photopolymerization. After breaking the glass vials, the product was placed into distilled water to remove NaAc and unreacted substances; XGH with aligned pores were finally obtained.

As a control, non-alighed XGH were also prepared. The process for non-aligned XGH preparation was similar to the procedures above without the additions of NaAc and $NaAc{\cdot}3H_2O$.

A series of aligned and non-aligned XGH were prepared by varying the dosages of components; a detailed feed composition is listed in Table 1.

Table 1. Specific Feed Composition of XGH with Aligned Pores

Sample No.	XG (g)	AM (g)	Gelatin (g)	Irgacure 2959 (g)	MBAA (mL)	DMSO (mL)	NaAc (g)	H_2O (mL)
1	0.3 (1.0%)	3.6 (12%)	0.3	0.108	0.9	6	21	23.1
2	0.3 (1.0%)	4.5 (15%)	0.3	0.135	1.125	6	21	22.875
3	0.3 (1.0%)	5.4 (18%)	0.3	0.162	1.35	6	21	22.650
4	0.3 (1.0%)	6.0 (20%)	0.3	0.180	1.5	6	21	22.500
5	0.15 (0.5%)	3.6 (12%)	0.3	0.108	0.9	6	21	23.1
6	0.45 (1.5%)	3.6 (12%)	0.3	0.108	0.9	6	21	23.1
7	0.60 (2.0 %)	3.6 (12%)	0.3	0.108	0.9	6	21	23.1

For the non-aligned hydrogels, all the above compounds in Table 1 were added except for NaAc; XG and AM concentrations (values in parenthesis) were based on w/v

Methods

Morphology study

Surface morphologies of XGH with aligned and non-aligned pores were analyzed using scanning electron microscopy (SEM) (Hitachi S 4800; Hitachi, Tokyo, Japan) with a field emission at an accelerating voltage of 3 kV. Before SEM analysis, the hydrogels were first quenched in liquid nitrogen; after freeze-drying, the samples were sputter-coated with a thin layer of gold using Magnetron Ion Sputter Metal Coating Device (MSP-2S; IXRF Systems, Inc., Japan) to make them electrically conductive.

Compression testing

Compression tests were performed with a tensile testing machine (FR-108C; Shanghai Farui Instrument Technology Co., Ltd., Shanghai, China) at a velocity of 1 mm/min. All samples were prepared as cylinders with a diameter of approximately 18 mm, and a height of approximately 10 mm as measured with a vernier caliper. The Young's compressive modulus was calculated from the slope of the stress-strain curve in the strain range of 5% to 15%. For each condition, at least three samples were tested to obtain an average compression modulus value.

Porosity and density measurement

The porosity and density of the XGH were evaluated according to a published liquid displacement method (Zhang and Ma 1999). The total volume of the hydrogel was divided into two parts: the volume of the hydrogel skeleton and the void volume. Specifically, a lyophilized hydrogel of mass m_0 (g) was immersed in a graduated cylinder containing a known volume (V_0, cm^3) of ethanol for 30 min. Next, evacuation-repressurization cycles were performed to enable the ethanol to penetrate completely into the pores of the hydrogel; the total volume of the ethanol and ethanol-soaked hydrogel was recorded as V_1 (cm^3). Hence, (V_1 - V_0) is considered as the volume of the hydrogel skeleton. Then, the gel was removed from the graduated cylinder, and the residue volume was recorded as V_2 (cm^3). Hence, (V_0 - V_2) is the volume of ethanol held in the hydrogel, which is supposed to be the void volume of the hydrogel. Therefore, the volume of the hydrogel, V (cm^3), should be:

$$V = (V_1 - V_0) + (V_0 - V_2) = V_1 - V_2 \quad (1)$$

The porosity (P, %) of the hydrogel can be calculated using Eq. 2,

$$P = (V_0 - V_2) \times 100\%/V = (V_0 - V_2) \times 100\%/(V_1 - V_2) \quad (2)$$

and the density (D, g/cm^3) of the hydrogel can be obtained according to Eq. 3:

$$D = m_0/V = m_0/(V_1 - V_2) \quad (3)$$

Simulated Body Fluid Absorption

The absorption properties of the XGH with and without oriented pores were determined using a simulated body fluid (SBF). The SBF solution, at 37 °C and pH 7.4 (buffered with tris(hydroxymethyl)aminomethane and 1 M hydrochloric acid) that contained 142 mM Na^+, 5.0 mM K^+, 2.5 mM Ca^{2+}, 148 mM Cl^-, 4.2 mM HCO_3^-, 1.0 mM HPO_4^{2-}, and 5.0 mM SO_4^{2-}, was prepared in the laboratory according to a previous method with minor differences (Ong *et al*. 2008). Each pre-weighed and dried hydrogel was immersed in 200 mL SBF and incubated at 37 °C. The sample was then taken out at pre-set time intervals and immediately weighed (W_t) after the removal of excess fluid on its surface with filter paper. The uptake capacity or absorption ratio (g/g) is calculated as,

$$\text{Absorption ratio} = (W_t - W_0)/W_0 \quad (4)$$

where W_0 is the initial dry mass of the hydrogel (g) and W_t is the mass of the hydrogel (g) incubated for time t (h).

Cytotoxicity

Mouse embryonic fibroblasts (NIH/3T3) were purchased from American Type Culture Collection (ATCC, Manassas, VA, USA). The cells were cultured in Dulbecco's modified eagle medium (DMEM) that contained 10% (v/v) fetal bovine serum (FBS) and 1% (v/v) penicillin-streptomycin in a humidified incubator at 37 °C with 5% CO_2. Before being co-cultured with the cells, the hydrogels were cut into small pieces and soaked in distilled water to remove residual sodium acetate. Afterward, the small pieces of hydrogel were sterilized using alcohol and ultraviolet lamp exposure for 4 h. Then, the hydrogels were immersed in ultra-pure water for another 4 h by changing the water every 30 min. To remove all the residual alcohol, the hydrogels were placed into a phosphate buffer solution for 24 h. Finally, the hydrogels were transferred to the DMEM medium containing 10% FBS and 1% penicillin-streptomycin. The cytotoxicity evaluation of the hydrogel was conducted *via* an MTT (3-(4,5-dimethylthiazol-2-yl)-2,5-diphenyl tetrazolium bromide) staining assay. First, the NIH/3T3 cells were seeded in 24-well plates and cultured for 24 h. Next, the hydrogels of different masses were added and co-cultured for another 12 h or 24 h. After changing the culture medium, 20 μL MTT solution was added to the well and cultured for another 4 h. Cell viability was measured using a microplate reader (Bio-Tek ElX800; Bio-Tek U.S., Winooski, VT, USA) at the wavelength of 570 nm after adding 200 μL Formazan dissolving liquid to each well in the plate.

RESULTS AND DISCUSSION

Construction of XGH with Aligned Structure

Figure 1 shows the general procedure for preparing the XGH with an oriented structure. The addition of DMSO was used in this process to promote the dissolution of XG. Gelatin was also added to the system to improve cell attachment. A series of XGH were prepared to investigate the influence of XG and AM proportions on the properties of the materials; detailed conditions for each hydrogel are given in Table 1.

Morphology of XGH

The morphological structures of aligned XGH were analyzed by SEM from different angles to get a comprehensive understanding. Figures 2a, 2b, and 2c show longitudinal, diagonal, and transverse sections of the freeze-dried aligned XGH, respectively. From Fig. 2a it can be observed that there were many parallel straight channels throughout the entire material, the pore diameters were approximately 10 μm (Figs. 2b and 2c). These results demonstrated that XGH with oriented structure was successfully prepared. This special morphology endowed XGH to be applied as electrolyte of all-solid-state supercapacitors. Aligned XGH could also be used as biological scaffolds to direct cell growth and mimic properties of some natural tissues.

As a control, non-aligned XGH also presented a three-dimensional network, but the interconnected pores were randomly arranged, and the pore size was much smaller than the aligned hydrogel (80 to 100 nm, Fig. 2d).

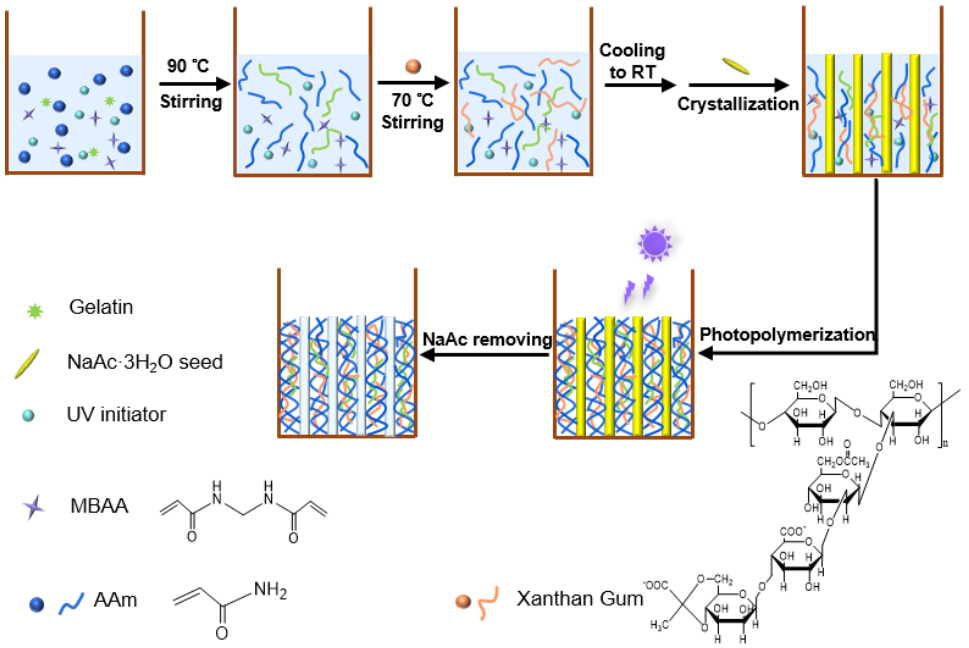

Fig. 1. Schematic for the preparation of XGH with aligned pores *via* sodium acetate trihydrate template and photopolymerization

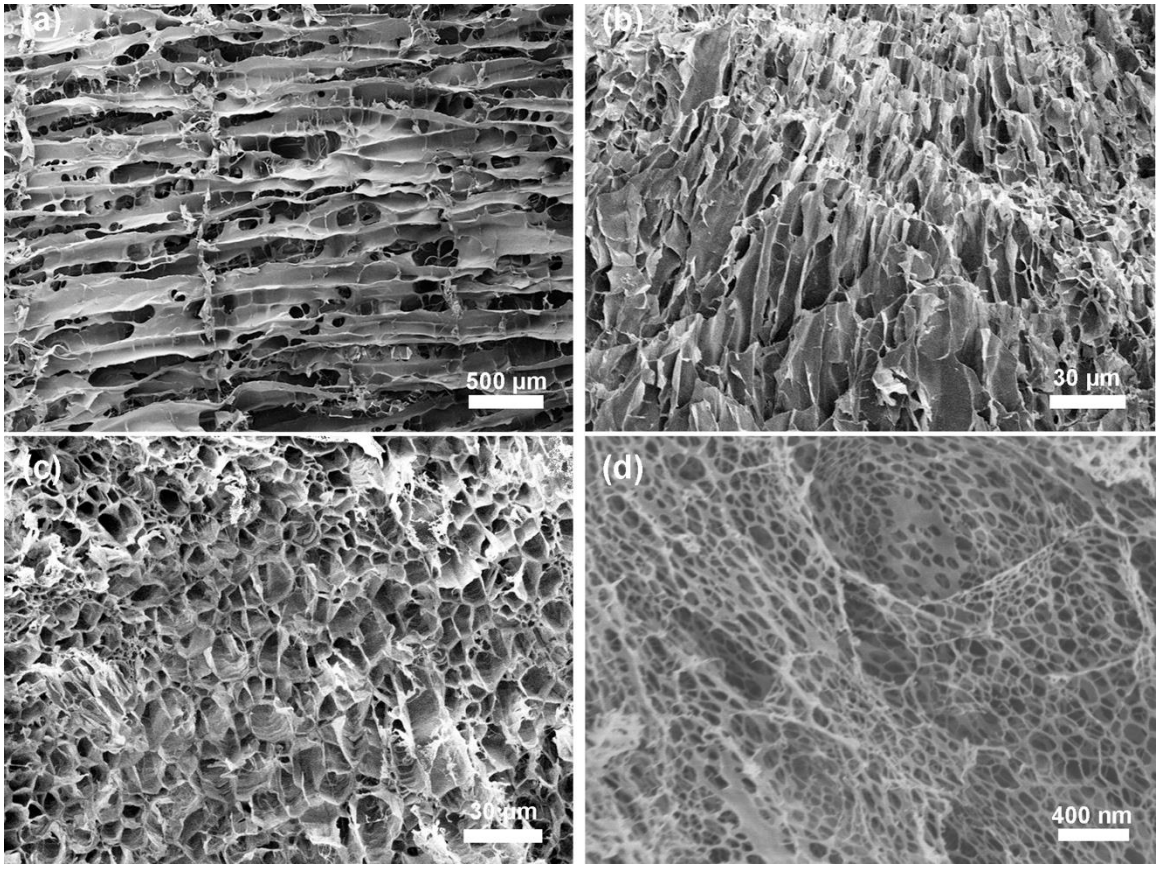

Fig. 2. SEM images of XGH: (a) to (c) longitudinal, diagonal, and transverse sections of the aligned hydrogel, respectively, and (d) image of non-aligned hydrogel with the same constituents as sample 6 except for the orientation process with NaAc. Sample 6 (Table 1; AM 12% and XG 1.5%) was used for SEM test.

Compressive Performance

Compressive tests were conducted to assess the mechanical properties of the XGH, as shown in Figs. 3 and 4, and in Tables 2 and 3. All of the aligned hydrogels tolerated a compression that was greater than 95% under the experimental conditions. Moreover, the compressive strength was enhanced for the aligned XGH as the AM and XG concentrations increased (Figs. 4a and 4b). The maximum compressive strength at a strain of 95% for the aligned XGH was 0.439 MPa (AM 20% and XG 1.0%).

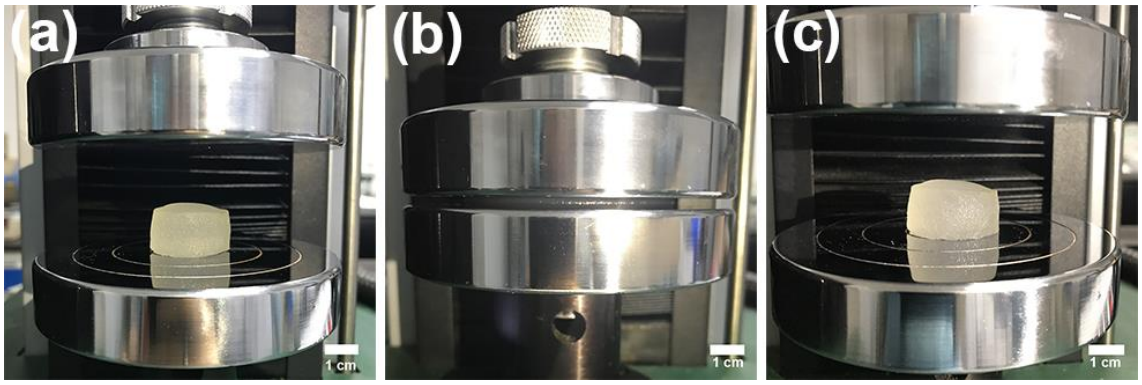

Fig. 3. Photographs of compressive strength testing of XGH with aligned structure: (a) before compression, (b) over 80% of the hydrogel is compressed, and (c) after compression

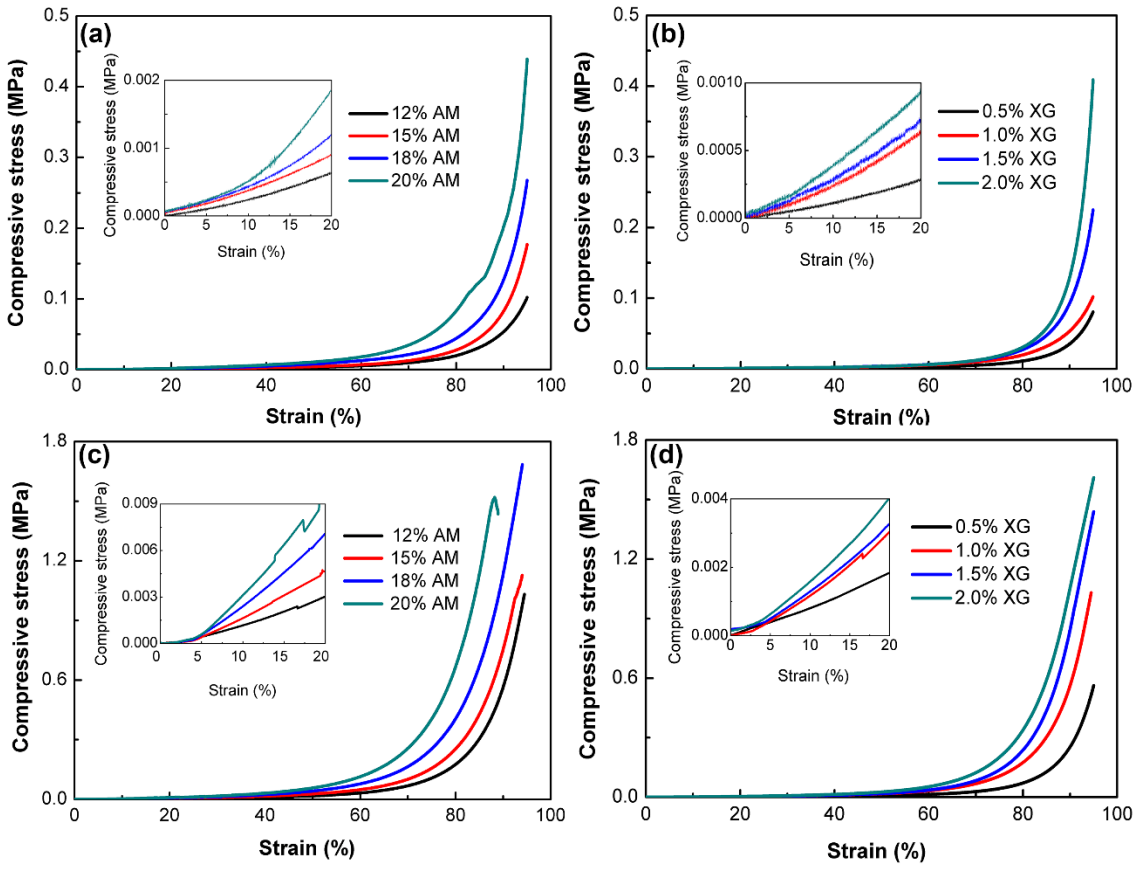

Fig. 4. Compression curves of XGH: (a) and (c) compressive strength of aligned and non-aligned XGH with different AM concentrations, respectively; (b) and (d) compressive strength of aligned and non-aligned XGH with different XG concentration, respectively

The compressive strengths of the non-aligned hydrogels were larger than the aligned hydrogels. As the AM concentration increased from 12% to 18%, the compressive strength increased from 1.031 to 1.685 MPa at a strain of 95%. However, a further increase of AM to 20% led to cracks in the hydrogel at a strain of 88.2% and a stress of 1.519 MPa (Fig. 4c). Compressive strengths for the non-aligned hydrogels also increased with the increase of XG concentration (Fig. 4d).

From Tables 2 and 3, the compressive moduli of the aligned XGH were much smaller than the non-aligned hydrogels, which indicated that the XGH after orientation were more flexible than the non-aligned hydrogels. The cyclic loading-unloading compression up to 95% strain was completed on an aligned XGH (Sample 6) to further investigate the fatigue resistance. The results are shown in Fig. 5. The compressive strength slightly decreased as the cyclic compression number increased. After 30 consecutive compression cycles, the compressive strength at a strain of 95% (0.581 MPa) remained 71.3% of the first cycle (0.816 MPa). The areas of hysteresis loops in loading-unloading curves indicate energy dissipation exists in the aligned XGH (Huang *et al*. 2007; Wei *et al*. 2015). However, the non-aligned hydrogels exhibit rigidity and cannot tolerate cyclic compression. Therefore, it can be concluded that the aligned structure endowed XGH with energy dissipation and hysteresis loops to resist crack propagation.

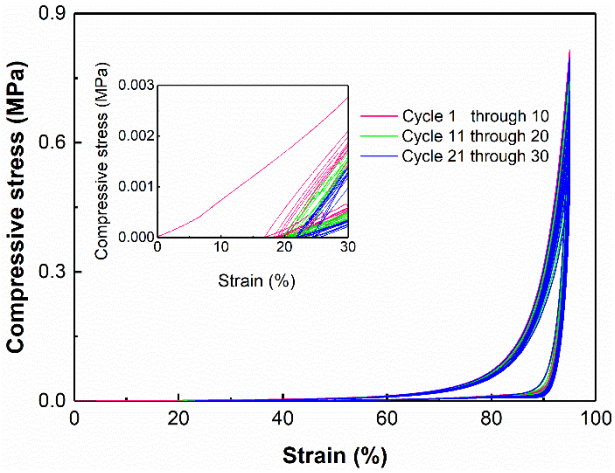

Fig. 5. Loading-unloading curves of cyclic compression test for aligned XGH (Sample 6)

Table 2. Compression Properties of XGH with Different AM Concentration

Sample No.	AM Conc.[a]	Compressive Modulus (MPa)		Compressive Strength (MPa)[b]	
		Aligned Hydrogel	Non-aligned Hydrogel	Aligned Hydrogel	Non-aligned Hydrogel
1	12%	0.00030 ± 0.00002	0.00164 ± 0.00008	0.102 ± 0.005	1.031 ± 0.052
2	15%	0.00042 ± 0.00002	0.00270 ± 0.00014	0.177 ± 0.009	1.127 ± 0.056
3	18%	0.00051 ± 0.00003	0.00403 ± 0.00020	0.267 ± 0.013	1.685 ± 0.074
4	20%	0.00083 ± 0.00004	0.00578 ± 0.00029	0.439 ± 0.022	—

[a] Conc. is concentration; for samples 1, 2, 3, and 4, the XG concentration was 1.0%;
[b] Compressive strength at a maximum strain of 95%

Table 3. Compression Properties of XGH with Different XG Concentration

Sample No.	XG Conc.[c]	Compressive Modulus (MPa)		Compressive Strength (MPa)[d]	
		Aligned Hydrogel	Non-aligned Hydrogel	Aligned Hydrogel	Non-aligned Hydrogel
5	0.5%	0.00014 ± 0.00001	0.00090 ± 0.00005	0.081 ± 0.004	0.563 ± 0.005
1	1.0%	0.00030 ± 0.00002	0.00164 ± 0.00008	0.102 ± 0.005	1.031 ± 0.052
6	1.5%	0.00036 ± 0.00002	0.00170 ± 0.00009	0.225 ± 0.012	1.439
7	2.0%	0.00047 ± 0.00003	0.00267 ± 0.00013	0.409 ± 0.021	1.609

[c] Conc. is concentration; for samples 1, 5, 6, and 7, the AM concentration was 12%;
[d] Compressive strength at a maximum strain of 95%

Porosity and Density

The porosity and density values of the freeze-dried XGH with aligned pores were studied; the results were compared with the non-aligned freeze-dried XGH prepared under the same condition as shown in Fig. 6. In Fig. 6a, as the AM increased from 12% to 20% for the aligned XGH, the porosity decreased from 94.9% to 88.8%, while for the non-aligned XGH, the porosity decreased from 88.9% to 81%. In Fig. 6b, when the XG increased from 0.5% to 2.0%, the porosity decreased from 95.4% and 90.0% to 90.9% and 80.2% for the aligned and non-aligned hydrogels, respectively.

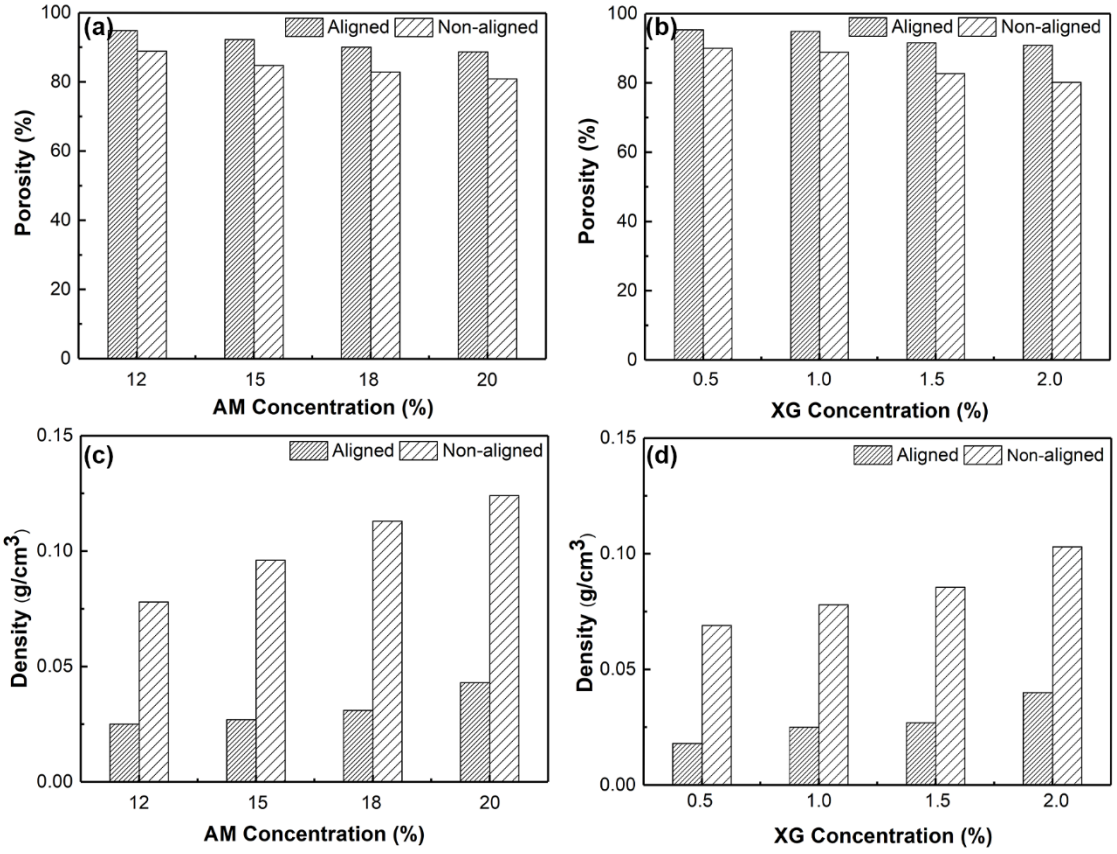

Fig. 6. Porosity and density of freeze-dried XGH: (a) and (c) porosity and density for freeze-dried XGH with and without aligned pores with the variation of AM concentration, respectively, referred to sample 1, 2, 3, and 4 in Table 1, (b) and (d) porosity and density for freeze-dried XGH with and without aligned pores with the variation of XG concentration, respectively, referred to sample 1, 5, 6, and 7 in Table 1

In Fig. 6c, when the AM increased from 12% to 20%, the density increased from 0.025 and 0.078 g/cm^3 to 0.043 and 0.124 g/cm^3 for the aligned and non-aligned hydrogels, respectively. In Fig. 6d, when XG increased from 0.5% to 2.0%, the density increased from 0.018 and 0.069 g/cm^3 to 0.4 and 0.103 g/cm^3, respectively. The variations of the porosity and the density of the hydrogels were attributed to the differences in the degree of cross-linking. Higher polymer concentrations led to a higher cross-linking degree; therefore, the hydrogels prepared with high polymer concentrations tended to have low porosity and high density.

In Fig. 6, it can also be seen that aligned XGH had higher porosity and lower density when compared to the non-aligned hydrogels with the same polymer concentration. Due to the effect of sodium acetate crystals, aligned hydrogels had straight channels, and the pore sizes of aligned hydrogels were much larger than the non-aligned hydrogels, therefore, higher porosities were observed.

SBF Absorption Capacity

The swelling ability of the dried XGH was evaluated by soaking the hydrogels in SBF. The results are shown in Fig. 7.

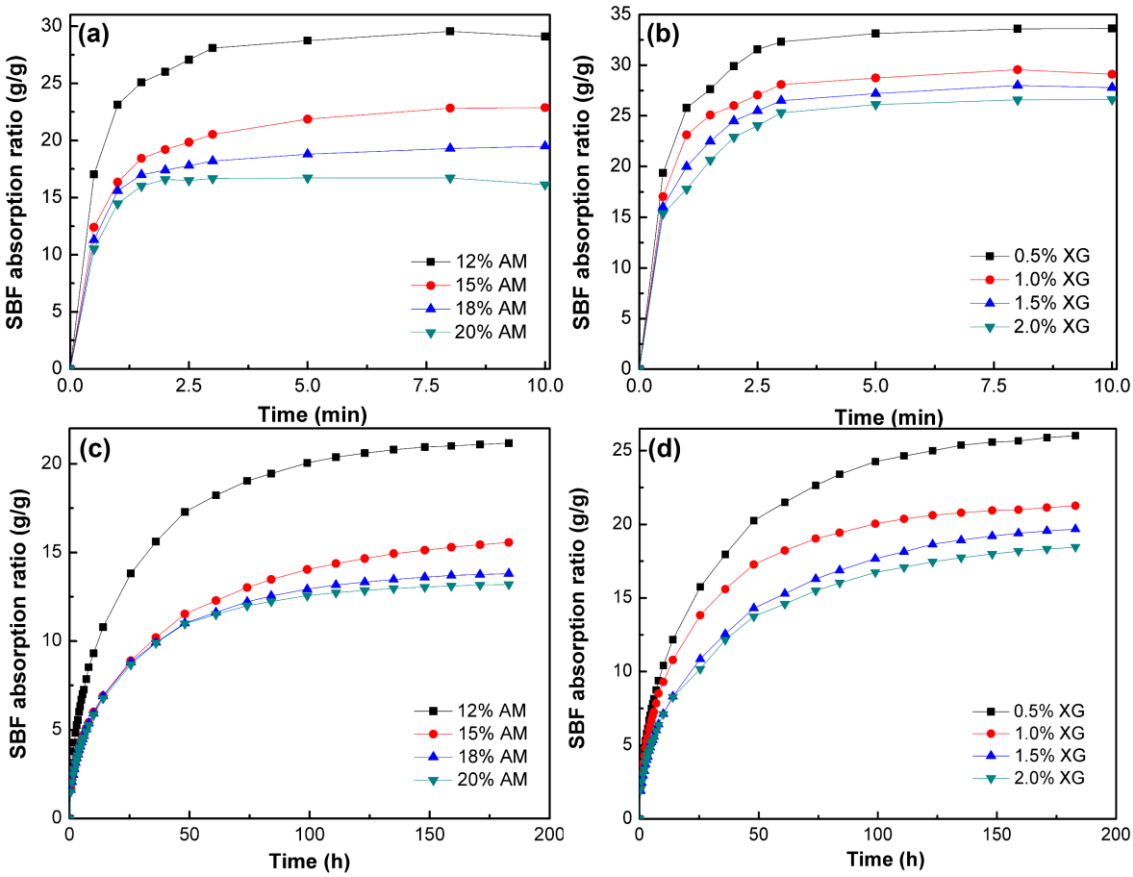

Fig. 7. SBF absorption capacities of dried XGH with and without aligned structure: (a) and (c) SBF capacity of aligned and non-aligned XGH with different AM concentration, respectively, (b) and (d) SBF capacities of aligned and non-aligned XGH with different XG concentrations, respectively

During the tested incubation periods, the absorbing capacities of all hydrogels increased as the soaking time increased, and decreased as the AM and XG concentrations increased. In Figs. 7a and 7c, when the AM concentration increased from 12% to 20%, the equilibrium absorption ratio decreased from 29.1 and 20.9 to 16.1 and 13.0, for the aligned and non-aligned hydrogels, respectively. In Figs. 7b and 7d, when the XG increased from 0.5% to 2.0%, the equilibrium absorption ratio decreased from 33.6 and 25.6 to 22.6 and 18.0, for the aligned and non-aligned hydrogels, respectively. A higher polymer concentration resulted in a denser three-dimensional network of the hydrogel, which led to a lower absorption capacity for the material.

The equilibrium absorption ratio of aligned hydrogels was higher than the corresponding non-aligned hydrogels; this was because the aligned hydrogels had higher porosity, as illustrated in Fig. 6. Moreover, the aligned XGH exhibited a much higher absorption rate than the non-aligned hydrogels. Absorption equilibria were attained within the first 5 min for all the aligned hydrogels, while more than 100 h were required for the non-aligned samples. The results indicated that the large pore size and the straight porous structure were more favorable for small molecules or ions to penetrate into the hydrogel. Therefore, it can be concluded that the aligned XGH are more suitable to absorb a large quantity of liquid in a short time. Combined with the porosity measurement, XGH can be used as a potential wound dressing material with favorable air permeability and liquid adsorption performance, whereas the non-aligned hydrogels can be applied to absorb excessive exudates over a long time.

Biocompatibility

The initial biocompatibilities of XGH were evaluated by the incubation of NIH/3T3 cells for 12 h or 24 h at varying concentrations. The results are shown in Fig. 8. The cell viability of all the experimental groups was similar to the control group (without XGH). Even when the concentration of XGH increased from 10 mg/mL to 200 mg/mL, cell viability reached 92% after incubation for 24 h with the NIH/3T3 cells. These results demonstrated that the XGH was non-toxic, and can be applied to tissue engineering as bioscaffolds.

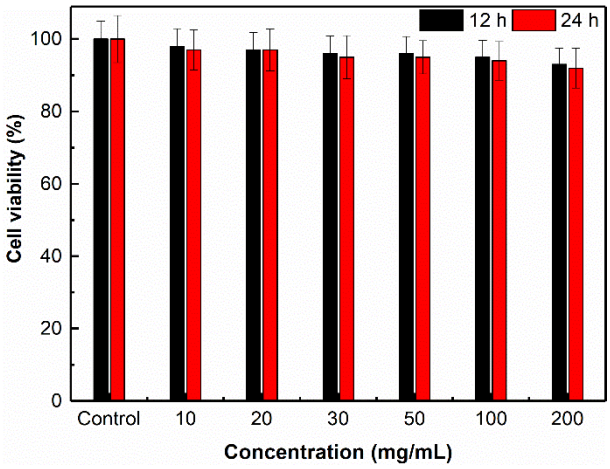

Fig. 8. Viability of NIH/3T3 cells after incubation with XG-AM hydrogels for 12 h or 24 h; each column was the average of 5 individual experiments. Sample 6 was used for cytotoxicity evaluation.

CONCLUSIONS

1. Aligned xanthan gum-based hydrogels (XGH) were successfully fabricated using sodium acetate crystals as template. The diameter of the straight internal channels was approximately 10 μm for hydrogel prepared with 12% AM and 1.5% XG, whereas the non-aligned hydrogels exhibited a much smaller pore size with the same polymer concentration.
2. The XGH with aligned structure were much more flexible than the non-aligned hydrogels. The maximum compressive strength for aligned XGH was 0.439 MPa at a strain of 95%.
3. Porosities of the freeze-dried aligned XGH were higher than the freeze-dried non-aligned XGH. Accordingly, the simulated body fluid (SBF) absorption capacity of the freeze-dried aligned XGH was also higher than the non-aligned XGH. It only took 5 min for the aligned samples to achieve absorption equilibrium, which was much faster than the 100 h for the non-aligned hydrogels.
4. The desirable biocompatibility of XGH was confirmed by cytotoxicity tests.

ACKNOWLEDGMENTS

This work was financially supported by the National Natural Science Foundation of China (No. 21878070), the Open Fund from State Key Laboratory of Pulp and Paper Engineering (No. 201807), the Program for Young Talents of Hubei Provincial Education Department (No. Q20181404), the Open Fund of Hubei Provincial Key Laboratory of Green Materials for Light Industry (No. 201710A07), the Doctoral Scientific Research Foundation of Hubei University of Technology (No. BSQD12135), and the Innovation and Entrepreneurship Training Program for College Students (S201910500038).

REFERENCES CITED

Anjum, F., Bukhari, S. A., Siddique, M., Shahid, M., Potgieter, J. H., Jaafar, H. Z., Ercisli, S., and Zia-Ul-Haq, M. (2015). "Microwave irradiated copolymerization of xanthan gum with acrylamide for colonic drug delivery," *BioResources* 10(1), 1434-1451. DOI: 10.15376/biores.10.1.1434-1451

Barrow, M., and Zhang, H. (2013). "Aligned porous stimuli-responsive hydrogels *via* directional freezing and frozen UV initiated polymerization," *Soft Matter* 9(9), 2723-2729. DOI: 10.1039/c2sm27722k

Bellini, M. Z., Pires, A. L. R., Vasconcelos, M. O., and Moraes, A. M. (2012). "Comparison of the properties of compacted and porous lamellar chitosan–xanthan membranes as dressings and scaffolds for the treatment of skin lesions," *Journal of Applied Polymer Science* 125(S2), E421-E431. DOI: 10.1002/app.36693

Chen, C., Tang, J., Gu, Y., Liu, L., Liu, X., Deng, L., Martins, C., Sarmento, B., Cui, W., and Chen, L. (2019). "Bioinspired hydrogel electrospun fibers for spinal cord regeneration," *Advanced Functional Materials* 29(4), Article ID 1806899. DOI: 10.1002/adfm.201806899

Drury, J. L., and Mooney, D. J. (2003). "Hydrogels for tissue engineering: Scaffold design variables and applications," *Biomaterials* 24(24), 4337-4351. DOI: 10.1016/s0142-9612(03)00340-5

Fan, J., Wang, K., Liu, M., and He, Z. (2008). "*In vitro* evaluations of konjac glucomannan and xanthan gum mixture as the sustained release material of matrix tablet," *Carbohydrate Polymers* 73(2), 241-247. DOI: 10.1016/j.carbpol.2007.11.027

García-Ochoa, F., Santos, V. E., Casas, J. A., and Gómez, E. (2000). "Xanthan gum: Production, recovery, and properties," *Biotechnology Advances* 18(7), 549-579. DOI: 10.1016/S0734-9750(00)00050-1

He, H., Liu, M., Wei, J., Chen, P., Wang, S., and Wang, Q. (2016). "Hydrogel with aligned and tunable pore *via* "hot ice" template applies as bioscaffold," *Advanced Healthcare Materials* 5(6), 648-652. DOI: 10.1002/adhm.201500707

Hoffman, A. S. (2012). "Hydrogels for biomedical applications," *Advanced Drug Delivery Reviews* 64(Supplement), 18-23. DOI: 10.1016/j.addr.2012.09.010

Huang, T., Xu, H. G., Jiao, K. X., Zhu, L. P., Brown, H. R., and Wang, H. L. (2007). "A novel hydrogel with high mechanical strength: A macromolecular microsphere composite hydrogel," *Advanced Materials* 19(12), 1622-1626. DOI: 10.1002/adma.200602533

Katzbauer, B. (1998). "Properties and applications of xanthan gum," *Polymer Degradation and Stability* 59(1-3), 81-84. DOI: 10.1016/s0141-3910(97)00180-8

Kumar, A., Rao, K. M., and Han, S. S. (2018). "Application of xanthan gum as a polysaccharide in tissue engineering: A review," *Carbohydrate Polymers* 180, 128-144. DOI: 10.1016/j.carbpol.2017.10.009

Lachke, A. (2004). "Xanthan – A versatile gum," *Resonance* 9(10), 25-33. DOI: 10.1007/bf02834866

Lian, Y., Zhang, J., Li, N., and Ping, Q. (2018). "Preparation of hemicellulose-based hydrogel and its application as an adsorbent towards heavy metal ions," *BioResources* 13(2), 3208-3218. DOI: 10.15376/biores.13.2.3208-3218

Liu, X., Wang, B., Jin, Z., Wang, H., and Wang, Q. (2015). "Elastic ionogels with freeze-aligned pores exhibit enhanced electrochemical performances as anisotropic electrolytes of all-solid-state supercapacitors," *Journal of Materials Chemistry A* 3(30), 15408-15412. DOI: 10.1039/c5ta03184b

Muller, G., Aurhourrache, M., Lecourtier, J., and Chauveteau, G. (1986). "Salt dependence of the conformation of a single-stranded xanthan," *International Journal of Biological Macromolecules* 8(3), 167-172. DOI: 10.1016/0141-8130(86)90021-8

Ong, S.-Y., Wu, J., Moochhala, S. M., Tan, M.-H., and Lu, J. (2008). "Development of a chitosan-based wound dressing with improved hemostatic and antimicrobial properties," *Biomaterials* 29(32), 4323-4332. DOI: 10.1016/j.biomaterials.2008.07.034

Petri, D. F. (2015). "Xanthan gum: A versatile biopolymer for biomedical and technological applications," *Journal of Applied Polymer Science*, 132(23), Article Number 42035. DOI: 10.1002/app.42035

Rochefort, W. E., and Middleman, S. (1987). "Rheology of xanthan gum: Salt, temperature, and strain effects in oscillatory and steady shear experiments," *Journal of Rheology* 31(4), 337-369. DOI: 10.1122/1.549953

Song, P., Wu, Y., Zhang, X., Yan, Z., Wang, M., and Xu, F. (2018). "Preparation of covalently crosslinked sodium alginate/hydroxypropyl methylcellulose pH-sensitive

microspheres for controlled drug release," *BioResources* 13(4), 8614-8628. DOI: 10.15376/biores.13.4.8614-8628

Wei, J., Wang, J., Su, S., Wang, S., and Qiu, J. (2015). "Tough and fully recoverable hydrogels," *Journal of Materials Chemistry B* 3(26), 5284-5290.

Wichterle, O., and Lim, D. (1960). "Hydrophilic gels for biological use," *Nature* 185(4706), 117-118. DOI: 10.1038/185117a0

Zhang, R., and Ma, P. X. (1999). "Poly(α-hydroxyl acids)/hydroxyapatite porous composites for bone-tissue engineering. I. Preparation and morphology," *Journal of Biomedical Materials Research* 44(4), 446-455. DOI: 10.1002/(sici)1097-4636(19990315)44:4<446::aid-jbm11>3.0.co;2-f

Article submitted: December 13, 2019; Peer review completed: March 9, 2020; Revised version received and accepted: May 14, 2020; Published: May 29, 2020.
DOI: 10.15376/biores.15.3.5627-5640